Supplementary Information: Simulation of the Non-Adiabatic Dynamics of an Enone-Lewis Acid Complex in an Explicit Solvent

Martin T. Peschel,[a] Jörg Kussmann,[a], Christian Ochsenfeld[a,b] and Regina de Vivie-Riedle[a]

[a] *Department of Chemistry, Ludwig-Maximilians-Universität München (LMU), Butenandtstr. 5–13, D-81377 Munich, Germany*

[b] *Max-Planck-Institute for Solid State Research, Heisenbergstr. 1, D-70569 Stuttgart, Germany*

E-Mail: christian.ochsenfeld@cup.uni-muenchen.de

1 TDDFT benchmarks

The fast dissociation of the complex takes place mainly in S_1, thus, the most important figure of merit that a density functional should reproduce is the excited state gradient in S_1, ∇E_1. Apart from the gradient ∇E_1, two other parameters are considered when choosing the density functional; 1) the S_0S_1 energy gap ΔE_{01}, relevant for the selection of initial geometries based on the calculated absorption spectrum; 2) the S_1S_2 energy gap ΔE_{12}, which might become relevant because the S_1 and S_2 states are energetically close in the FC region and thus S_2 might be transiently populated even after an initial excitation to S_1.

A benchmark set was explicitly constructed for 2-cyclohexenone-BF_3. From the short gas-phase dynamics presented in ref. 1, $N = 96$ geometries were randomly sampled. At these geometries, excitation energies and gradients were calculated at the XMS-CASPT2(8,7)/cc-pVQZ [2] level of theory. All XMS-CASPT2 calculations were performed using an (8,7) active space containing two π-orbitals (π_1, π_2), two π^*-orbitals (π_1^*, π_2^*), the oxygen lone pair n and the σ- and σ^*-orbitals of the α-C-C bond (see fig. S-1). The calculations employed state averaging over three states (S_0, S_1, S_2), the single-state-single-reference flavor of multistate CASPT2 and an imaginary shift of 0.2. The cc-pVQZ basis set [3] was used with the resolution of the identity approximation and the cc-pVQZ-jkfit auxiliary basis. The benchmark calculations were performed using the OpenMOLCAS [4] and BAGEL [5] programs.

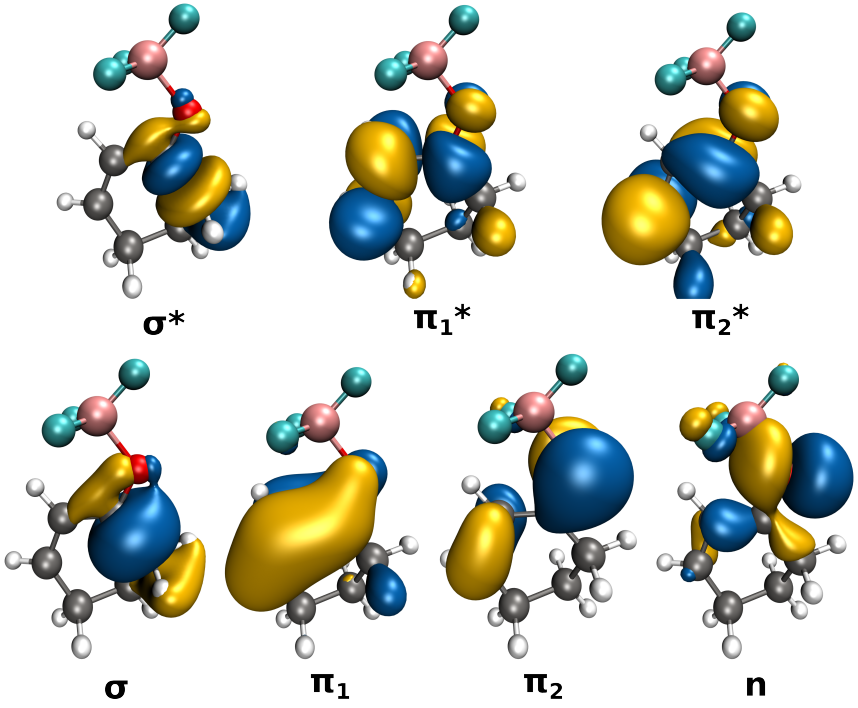

Figure S-1: Orbitals in the (8,7) active space of cyclohexenone-BF_3 (isovalue: 0.02).

There is a large number of DFT functionals available in the library LibXC. [6] Nearly all of them were tested (93 in total; some were excluded for technical reasons, see table S-2 for a list of all

tested functionals). Corrections due to dispersion (VV10[7], D3[8]) were also tested. Since the overall errors for energies and gradients in excited states are much larger than in the ground state, the resulting corrections were found to be negligible. Since the dynamics can be performed at most with a triple-zeta basis set due to computational costs, all DFT calculations were performed using the def2-TZVP basis set. The different functionals f were compared to the benchmark calculations on the three criteria of 1) S_1 gradients ∇E_1, 2) S_1S_2 energy gap ΔE_{12}, 3) S_0S_1 energy gap ΔE_{01}. The RMSD for each criterion x and each functional f were calculated according to

$$\mathrm{RMSD}(x, f) = \sqrt{\frac{\sum_i^N |x_i^f - x_i^{CASPT2}|^2}{N}}. \tag{1}$$

The RMSD values for each criterion x were shifted and scaled to obtain normalized values NRMSD(x, f). This was done so that the best ten functionals for that criterion covered the range between 0 and 1.

Then, a combined measure of error M was calculated as

$$\begin{aligned} M(f) = w_1 &\cdot \mathrm{NRMSD}(\nabla E_1, f) \\ + w_2 &\cdot \mathrm{NRMSD}(\Delta E_{12}, f) \\ + w_3 &\cdot \mathrm{NRMSD}(\Delta E_{01}, f) \end{aligned} \tag{2}$$

with weighting factors $\{w_i\}$ that sum to 1. These weighting factors encode the relative importance of the accurate description of each benchmarked criterion for the process under study. Different functionals perform best, depending on the choice of $\{w_i\}$. In fig. S-2, the best-performing functionals (minimal M) are shown, depending on w_1, w_2, and w_3. For all functionals that are best performing at any choice of $\{w_i\}$, the RMSD values for each criterion are given in table S-1, and the averages over all 93 tested functionals are shown in the last row. The exact RMSD values for all tested functionals can be found in the appendix (section 1).

The prediction of the S_1S_2 energy gap is the most difficult task with errors that are approximately a factor of three higher than for the S_0S_1 energy gap. The functionals PBE-MOL0[9] and B97-3[10] perform significantly better in the prediction of the S_1S_2 energy gap than all other functionals. Of these, PBE-MOL0 performs best for the S_0S_1 energy gap. Thus, the functional PBE-MOL0, a non-empirically improved version of PBE0 for molecular properties,[9] was chosen for the dynamics. It is the second-best for ΔE_{12}, the third-best for ΔE_{01}, and provides gradients significantly better than the average functional. We do not make generalizing conclusions about the performance of functionals in other circumstances (other properties, other molecules, or even different excited states of the same molecule) from our benchmark data. Even though our benchmark tests a lot of different functionals, it focuses on one specific excited state of a single molecule. Thus, significance for and transferability to other cases are exceedingly limited.

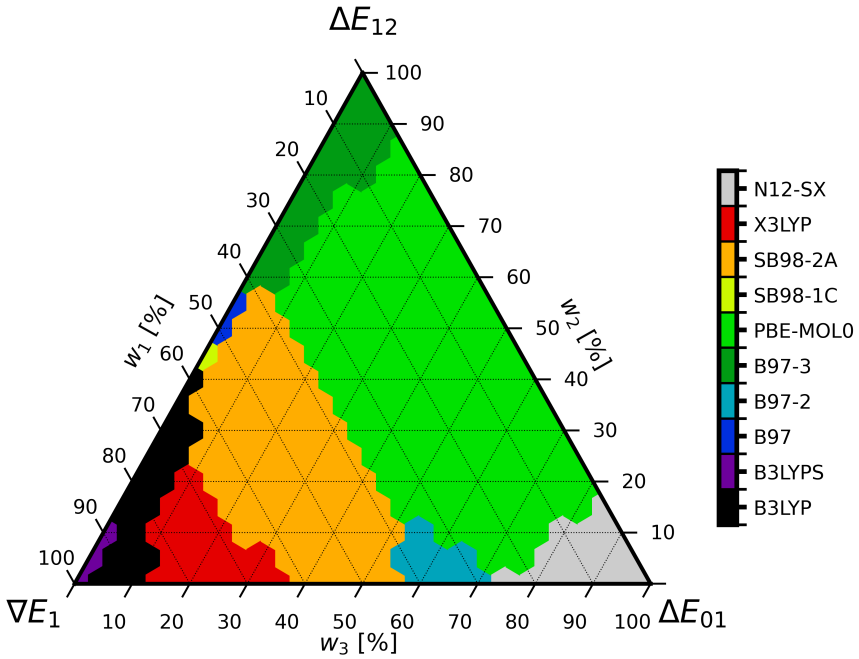

Figure S-2: Functionals with a minimal measure of error M according to eq. (2) for all different combinations of weights; weight w_1 for the gradient ∇E_1, weight w_2 for the S_0S_1 energy gap ΔE_{01}, and weight w_3 for the S_1S_2 energy gap ΔE_{12}

However, a more general benchmark of TDDFT excited state gradients and couplings on a variety of small to medium-sized organic molecules (for example, Thiel's benchmark set [11,12]) away from the FC region might be a worthwhile undertaking in the future since existing benchmarks focus heavily on equilibrium geometries. [13–15]

Table S-1: Performance of selected best performing functionals compared to XMS-CASPT2(8,7)/cc-pVQZ. The last row shows the average for all 93 tested functionals.

Functional	RMSD(∇E_1)	RMSD(ΔE_{01})	RMSD(ΔE_{12})
N12-SX	4.5786	0.1725	0.7267
X3LYP	4.3673	0.1773	0.7329
SB98-2A	4.4028	0.1753	0.7204
SB98-1C	4.3895	0.1953	0.7207
PBE-MOL0	4.5141	0.1733	0.7096
B97-3	4.5263	0.1811	0.7048
B97-2	4.4534	0.1740	0.7214
B97	4.3926	0.1939	0.7202
B3LYP	4.3367	0.1859	0.7325
B3LYPS	4.3186	0.2479	0.7509
Average	5.6960	0.3411	0.7873

Table S-2: Performance of all tested functionals compared to XMS-CASPT2(8,7)/cc-pVQZ.

Functional	RMSD(∇E_1)	RMSD(ΔE_{01})	RMSD(ΔE_{12})
APBE0	4.5314	0.1736	0.7109
APF	4.5197	0.1771	0.7158
B1LYP	4.4076	0.1796	0.7298
B1PW91	4.5500	0.1749	0.7122
B1WC	4.5950	0.2606	0.7463
B3LYP	4.3367	0.1859	0.7325
B3LYP3	4.3377	0.1862	0.7326
B3LYP5	4.3377	0.1862	0.7326
B3LYP-MCM1	4.3878	0.1959	0.7433
B3LYP-MCM2	4.5538	0.1739	0.7389
B3LYPS	4.3186	0.2479	0.7509
B3P86	4.4419	0.1928	0.7285
B3P86-NWCHEM	4.4528	0.1900	0.7286
B3PW91	4.4380	0.1932	0.7196
B5050LYP	5.7086	0.5538	0.8677
B97	4.3926	0.1939	0.7202
B97-1	4.4052	0.1837	0.7200
B97-1P	4.3759	0.2388	0.7333
B97-2	4.4534	0.1740	0.7214
B97-3	4.5263	0.1811	0.7048
B97-K	4.9029	0.3616	0.7495
BHANDH	6.3031	0.4925	0.8426
BHANDHLYP	5.6400	0.5575	0.8718
BLYP35	4.7566	0.2983	0.7586
CAM-B3LYP	5.0122	0.3252	0.7657

Continued on next page

Table S-2: Performance of all tested functionals compared to XMS-CASPT2(8,7)/cc-pVQZ. (Continued)

Functional	RMSD(∇E_1)	RMSD(ΔE_{01})	RMSD(ΔE_{12})
CAMH-B3LYP	4.6893	0.2438	0.7420
CAM-O3LYP	37.1717	1.1106	1.5859
CAM-PBEH	5.4353	0.3216	0.7875
CAM-QTP-00	6.9839	0.8142	1.0334
CAM-QTP-01	5.9665	0.5240	0.8520
CAM-QTP-02	6.3773	0.6135	0.8985
CAP0	4.6025	0.1752	0.7108
CASE21	4.5052	0.1736	0.7134
EDF2	4.4099	0.2186	0.7493
HAPBE	4.4381	0.1976	0.7186
HFLYP	10.1031	1.4713	1.5253
HPBEINT	4.5996	0.2533	0.7376
HSE03	4.5382	0.1735	0.7154
HSE06	4.5395	0.1747	0.7161
HSE12	4.7516	0.2059	0.7203
HSE12S	4.9283	0.2487	0.7291
HSE-SOL	4.8391	0.1822	0.7210
KMLYP	6.6171	0.6222	0.9019
LB07	6.8732	0.5454	0.8063
LC-BLYP	5.4560	0.3400	0.7741
LC-BLYP-EA	5.2215	0.2804	0.7669
LC-BLYPR	5.4216	0.3436	0.7634
LC-BOP	6.5177	0.6070	0.8533
LC-PBEOP	5.4328	0.3346	0.7544
LC-QTP	6.5925	0.6135	0.8695
LC-VV10	6.3408	0.5627	0.8051
LC-WPBE	5.9596	0.4686	0.7656
LC-WPBE08-WHS	6.3408	0.5627	0.8051
LC-WPBEH-WHS	6.7500	0.6758	0.8871
LC-WPBESOL-WHS	7.4771	0.8027	0.9645
LC-WPBE-WHS	5.9605	0.4694	0.7640
LRC-WPBE	5.1949	0.2690	0.7181
LRC-WPBEH	5.0020	0.2578	0.7334
MB3LYP-RC04	4.3698	0.1810	0.7319
MCAM-B3LYP	4.4916	0.1926	0.7303
MPW1K	5.4188	0.4027	0.7760
MPW1LYP	4.4127	0.1794	0.7342
MPW1PBE	4.5795	0.1748	0.7146
MPW1PW	4.5643	0.1749	0.7153
MPW3LYP	4.3686	0.1776	0.7357
MPW3PW	4.4494	0.1938	0.7233

Continued on next page

Table S-2: Performance of all tested functionals compared to XMS-CASPT2(8,7)/cc-pVQZ. (Continued)

Functional	RMSD(∇E_1)	RMSD(ΔE_{01})	RMSD(ΔE_{12})
MPWLYP1M	4.5101	0.4322	0.8801
O3LYP	4.3838	0.2905	0.7542
PBE0-13	4.9022	0.2436	0.7268
PBE-2X	6.3504	0.6247	0.8828
PBE38	5.1115	0.3056	0.7421
PBE50	5.9021	0.5183	0.8256
PBEB0	4.5604	0.1754	0.7195
PBEH	4.5878	0.1745	0.7148
PBE-MOL0	4.5141	0.1733	0.7096
PBE-MOLB0	4.4977	0.1749	0.7151
PBE-SOL0	4.8204	0.1777	0.7262
QTP17	7.0301	0.7262	0.9695
RCAM-B3LYP	6.2604	0.5920	0.8841
SB98-1A	4.6156	0.1770	0.7458
SB98-1B	4.4934	0.1921	0.7208
SB98-1C	4.3895	0.1953	0.7207
SB98-2A	4.4028	0.1753	0.7204
SB98-2B	4.4724	0.1763	0.7263
SB98-2C	4.4288	0.1778	0.7236
WB97	5.8680	0.5234	0.8285
WB97X	5.5078	0.4394	0.7998
WC04	10.4154	0.8560	1.0653
WHPBE0	20.3441	0.4801	0.8160
WP04	6.0977	0.1899	0.7554
X3LYP	4.3673	0.1773	0.7329
N12-SX	4.5786	0.1725	0.7267
SOGGA11-X	4.9354	0.3666	0.7592

2 Details of the kinetic model

The number of trajectories in Fig. 5 showing a C-C=O-B twist can be fit using a three-step kinetic model.

$$[A] \xrightarrow{\tau_1} [B] \xrightarrow{\tau_2} [C] \xrightarrow{\tau_3} [D] \tag{3}$$

The first step describes a delay in the onset of the C-C=O-B twist, which is caused by the initial fast O-B bond elongation, during which the kinetic energy of the dissociating complex is too high to observe a significant twisting motion. The second step describes the twisting of the C-C=O-B dihedral. The third step describes the un-twisting of the C-C=O-B dihedral due to ISC into the triplet states. Thus it should correspond to the ISC time of 1.8 ± 0.3 ps. We assume irreversible first-order kinetic for all steps.

$$\begin{aligned}
\frac{d[A]}{dt} &= -[A]/\tau_1 \\
\frac{d[B]}{dt} &= +[A]/\tau_1 \\
\frac{d[B]}{dt} &= -[B]/\tau_2 \\
\frac{d[C]}{dt} &= +[B]/\tau_2 \\
\frac{d[C]}{dt} &= -[C]/\tau_3 \\
\frac{d[D]}{dt} &= +[C]/\tau_3
\end{aligned} \tag{4}$$

Integration and fitting using the SciPy library[16] (initial conditions $[A](t_0) = 1, [B](t_0) = 0, [C](t_0) = 0, [D](t_0) = 0$) yields the time constants in table S-3.

Table S-3: Results of the kinetic model fit.

Parameter	Value
τ_1	0.06 ps
τ_2	0.16 ps
τ_3	1.57 ps

3 Time-resolved spectra

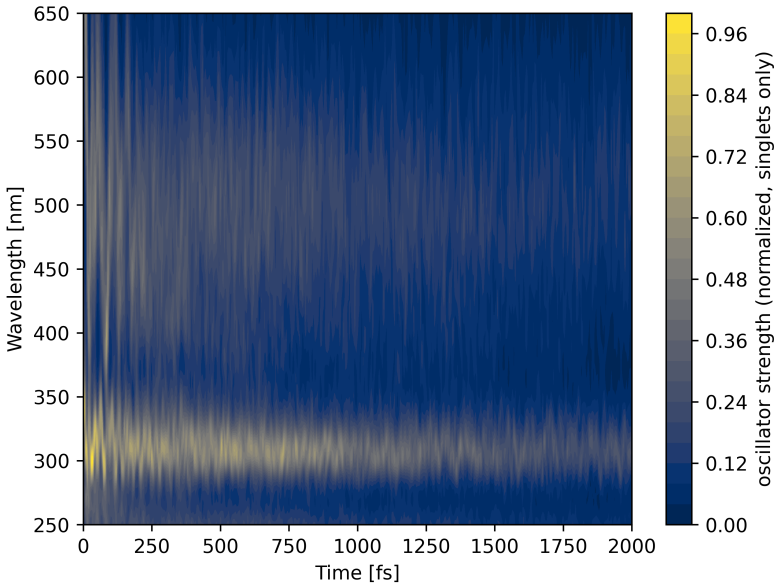

Figure S-3: Oscillator strengths for transitions originating in all active states during the trajectories. Time-resolved spectra were calculated at the PBEmol0/def2-TZVP level of theory using 30 singlet states. Geometries for the spectra calculation were sampled from the trajectories including triplet states at 10 fs intervals. Spectra were broadened with Gaussians ($\sigma = 0.1$ eV).

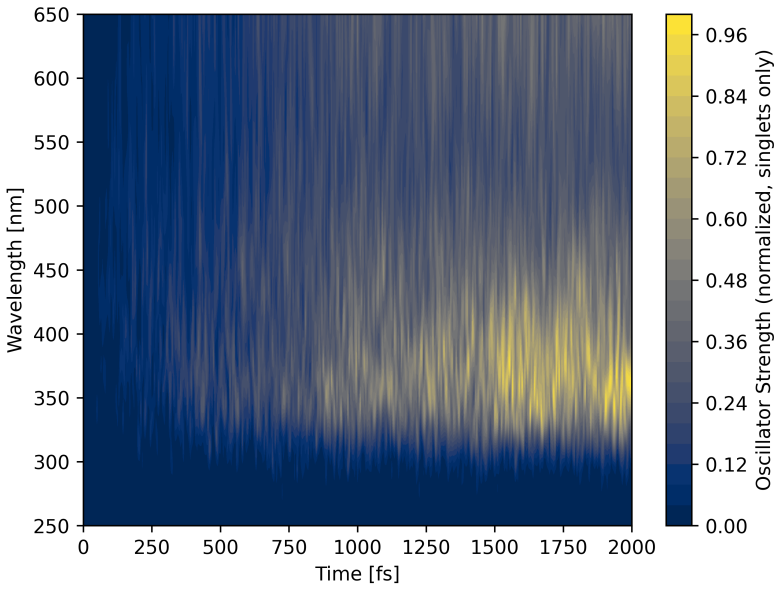

Figure S-4: Oscillator strengths for transitions originating in all active states during the trajectories. Time-resolved spectra were calculated at the PBEmol0/def2-TZVP level of theory using 30 triplet states. Geometries for the spectra calculation were sampled from the trajectories including triplet states at 10 fs intervals. Spectra were broadened with Gaussians ($\sigma = 0.1$ eV).

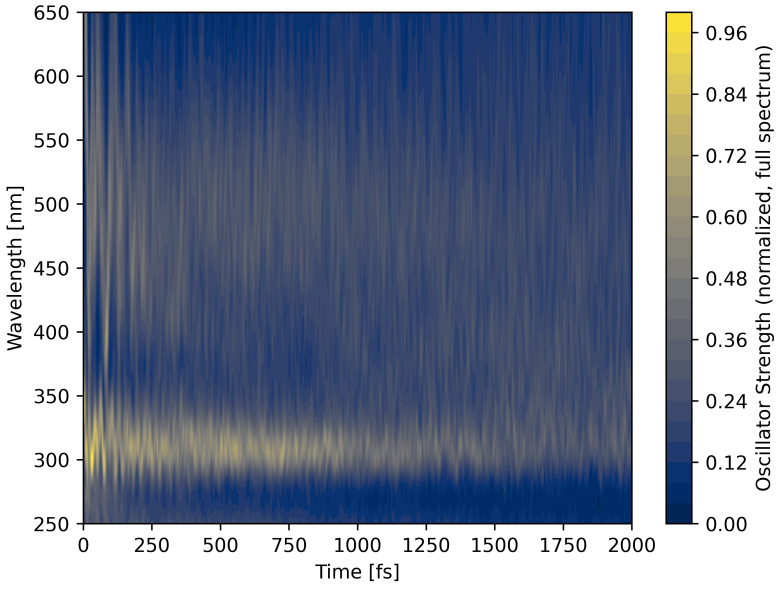

Figure S-5: Oscillator strengths for transitions originating in all active states during the trajectories. Time-resolved spectra were calculated at the PBEmol0/def2-TZVP level of theory using 30 singlet and 30 triplet states. Geometries for the spectra calculation were sampled from the trajectories including triplet states at 10 fs intervals. Spectra were broadened with Gaussians ($\sigma = 0.1$ eV).

4 Software for visualization and plotting

Molecular visualizations (structures, orbitals) in this work were created using VMD 1.9.3.[17,18] Plots were generated using Matplotlib 3.7.1.[19] Figures 2, 3, 5, and S-1 were assembled using Inkscape 1.3.[20]

References

[1] Martin T. Peschel, Piotr Kabaciński, Daniel P. Schwinger, Erling Thyrhaug, Giulio Cerullo, Thorsten Bach, Jürgen Hauer, and Regina de Vivie-Riedle. Activation of 2-Cyclohexenone by BF_3 Coordination: Mechanistic Insights from Theory and Experiment. *Angewandte Chemie International Edition*, 60(18):10155–10163, 2021.

[2] Toru Shiozaki, Werner Győrffy, Paolo Celani, and Hans-Joachim Werner. Communication: Extended multi-state complete active space second-order perturbation theory: Energy and nuclear gradients. *Journal of Chemical Physics*, 135(8):081106, 8 2011.

[3] Jr. Dunning, Thom H. Gaussian basis sets for use in correlated molecular calculations. I. The atoms boron through neon and hydrogen. *The Journal of Chemical Physics*, 90(2):1007–1023, 01 1989.

[4] Francesco Aquilante, Jochen Autschbach, Alberto Baiardi, Stefano Battaglia, Veniamin A. Borin, Liviu F. Chibotaru, Irene Conti, Luca De Vico, Mickaël Delcey, Ignacio Fdez Galván, Nicolas Ferré, Leon Freitag, Marco Garavelli, Xuejun Gong, Stefan Knecht, Ernst D. Larsson, Roland Lindh, Marcus Lundberg, Per Åke Malmqvist, Artur Nenov, Jesper Norell, Michael Odelius, Massimo Olivucci, Thomas B. Pedersen, Laura Pedraza-González, Quan M. Phung, Kristine Pierloot, Markus Reiher, Igor Schapiro, Javier Segarra-Martí, Francesco Segatta, Luis Seijo, Saumik Sen, Dumitru Claudiu Sergentu, Christopher J. Stein, Liviu Ungur, Morgane Vacher, Alessio Valentini, and Valera Veryazov. Modern quantum chemistry with [Open]Molcas. *Journal of Chemical Physics*, 152:214117, 2020.

[5] Toru Shiozaki. BAGEL: Brilliantly Advanced General Electronic-structure Library. *Wiley Interdisciplinary Reviews: Computational Molecular Science*, 8(1):e1331, 1 2018.

[6] Susi Lehtola, Conrad Steigemann, Micael J.T. Oliveira, and Miguel A.L. Marques. Recent developments in libxc – A comprehensive library of functionals for density functional theory. *SoftwareX*, 7:1–5, 1 2018.

[7] Oleg A. Vydrov and Troy Van Voorhis. Nonlocal van der Waals density functional: The simpler the better. *Journal of Chemical Physics*, 133(24):244103, 12 2010.

[8] Stefan Grimme, Jens Antony, Stephan Ehrlich, and Helge Krieg. A consistent and accurate *ab initio* parametrization of density functional dispersion correction (DFT-D) for the 94 elements H-Pu. *Journal of Chemical Physics*, 132(15):154104, 4 2010.

[9] Jorge M. del Campo, José L. Gázquez, S. B. Trickey, and Alberto Vela. Non-empirical improvement of PBE and its hybrid PBE0 for general description of molecular properties. *Journal of Chemical Physics*, 136(10):104108, 3 2012.

[10] Thomas W. Keal and David J. Tozer. Semiempirical hybrid functional with improved performance in an extensive chemical assessment. *Journal of Chemical Physics*, 123(12):121103, 9 2005.

[11] Marko Schreiber, Mario R. Silva-Junior, Stephan P. A. Sauer, and Walter Thiel. Benchmarks for electronically excited states: CASPT2, CC2, CCSD, and CC3. *Journal of Chemical Physics*, 128(13):134110, 4 2008.

[12] Mario R. Silva-Junior, Marko Schreiber, Stephan P. A. Sauer, and Walter Thiel. Benchmarks for electronically excited states: Time-dependent density functional theory and density functional theory based multireference configuration interaction. *Journal of Chemical Physics*, 129(10):104103, 9 2008.

[13] Jun Wang and Bo Durbeej. How accurate are TD-DFT excited-state geometries compared to DFT ground-state geometries? *Journal of Computational Chemistry*, 41(18):1718–1729, 7 2020.

[14] Amjad Ali, Muhammad Imran Rafiq, Zhuohan Zhang, Jinru Cao, Renyong Geng, Baojing Zhou, and Weihua Tang. TD-DFT benchmark for UV-visible spectra of fused-ring electron acceptors using global and range-separated hybrids. *Physical Chemistry Chemical Physics*, 22(15):7864–7874, 2020.

[15] Rudraditya Sarkar, Martial Boggio-Pasqua, Pierre-François Loos, and Denis Jacquemin. Benchmarking TD-DFT and Wave Function Methods for Oscillator Strengths and Excited-State Dipole Moments. *Journal of Chemical Theory and Computation*, 17(2):1117–1132, 2 2021.

[16] Pauli Virtanen, Ralf Gommers, Travis E. Oliphant, Matt Haberland, Tyler Reddy, David Cournapeau, Evgeni Burovski, Pearu Peterson, Warren Weckesser, Jonathan Bright, Stéfan J. van der Walt, Matthew Brett, Joshua Wilson, K. Jarrod Millman, Nikolay Mayorov, Andrew R. J. Nelson, Eric Jones, Robert Kern, Eric Larson, C J Carey, İlhan Polat, Yu Feng, Eric W. Moore, Jake VanderPlas, Denis Laxalde, Josef Perktold, Robert Cimrman, Ian Henriksen, E. A. Quintero, Charles R. Harris, Anne M. Archibald, Antônio H. Ribeiro, Fabian Pedregosa, Paul van Mulbregt, and SciPy 1.0 Contributors. SciPy 1.0: Fundamental Algorithms for Scientific Computing in Python. *Nature Methods*, 17:261–272, 2020.

[17] William Humphrey, Andrew Dalke, and Klaus Schulten. VMD – Visual Molecular Dynamics. *Journal of Molecular Graphics*, 14:33–38, 1996.

[18] John Stone. *An Efficient Library for Parallel Ray Tracing and Animation.* Master's thesis, Computer Science Department, University of Missouri-Rolla, April 1998.

[19] Thomas A Caswell, Antony Lee, Elliott Sales de Andrade, Michael Droettboom, Tim Hoffmann, Jody Klymak, John Hunter, Eric Firing, David Stansby, Nelle Varoquaux, Jens Hedegaard Nielsen, Benjamin Root, Ryan May, Oscar Gustafsson, Phil Elson, Jouni K. Seppänen, Jae-Joon Lee, Darren Dale, hannah, Damon McDougall, Andrew Straw, Paul Hobson, Kyle Sunden, Greg Lucas, Christoph Gohlke, Adrien F. Vincent, Tony S Yu, Eric Ma, Steven Silvester, and Charlie Moad. matplotlib/matplotlib: Rel: v3.7.1, March 2023.

[20] Inkscape Project. Inkscape: Rel: v1.3, July 2023.